analytical chemistry

Article

pubs.acs.org/ac

Overcoming Low Ge Ionization and Erosion Rate Variation for Quantitative Ultralow Energy Secondary Ion Mass Spectrometry Depth Profiles of $Si_{1-x}Ge_x$/Ge Quantum Well Structures

Richard J. H. Morris,* Mark G. Dowsett, Richard Beanland, Andrew Dobbie, Maksym Myronov, and David R. Leadley

Department of Physics, University of Warwick, Gibbet Hill Road, Coventry, CV4 7AL, U.K.

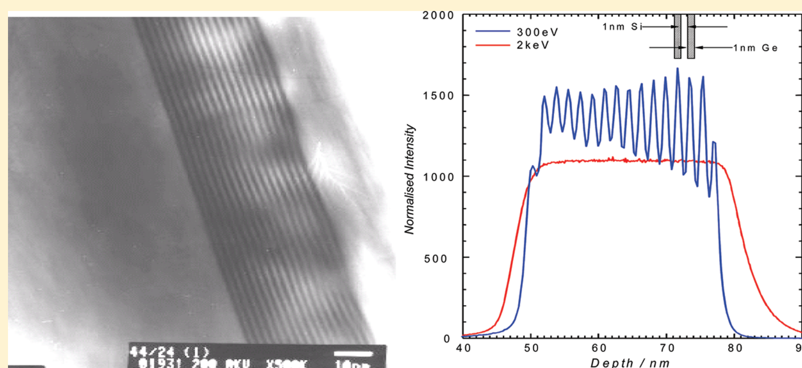

ABSTRACT: We specify the O_2^+ probe conditions and subsequent data analysis required to obtain high depth resolution secondary ion mass spectrometry profiles from multiple Ge/$Si_{1-x}Ge_x$ quantum well structures ($0.6 \leq x \leq 1$). Using an O_2^+ beam at normal incidence and with energies >500 eV, we show that the measured Ge signal is not monotonic with concentration, the net result being an unrepresentative and unquantifiable depth profile. This behavior is attributed to a reduced Ge ionization rate as x approaches 1. At lower beam energies the signal behaves monotonically with Ge fraction, indicating that the Ge atoms are now ionizing more readily for the whole range of x, enabling quantitative profiles to be obtained. To establish the depth scale a point-by-point approach based on previously determined erosion rates as a function of x is shown to produce quantum well thicknesses in excellent agreement with those obtained using transmission electron microscopy. The findings presented here demonstrate that to obtain reliable quantitative depth profiles from Ge containing samples requires O_2^+ ions below 500 eV and correct account to be taken of the erosion rate variation that exists between layers of different matrix composition.

To achieve quantifiable secondary ion mass spectrometry (SIMS) depth profiles with the best depth resolution, i.e., nanometer−subnanometer scale, it is important to start with an atomically smooth surface, retain this during sputtering, and understand how ion yields and erosion rates vary as a function of matrix concentration. The sputtering which is essential to SIMS as a method of analysis arises from the energy and momentum deposited by the primary ions in the top few nanometers of the sample.[1] Inevitably, this is accompanied by subsurface relocation and surface migration of component atoms[2] and the acquisition of probe material. The first effect destroys to some extent the original elemental distribution prior to its component atoms and molecules being sputtered out, the second can lead to the generation of surface topography such as ripples,[3] and the third alters the sample chemistry and electronic structure, further modifying the original distribution (through density renormalization and segregation[4]), enhancing or suppressing topographic effects (depending on other factors such as incident angle), but hugely increasing the secondary ion yields and therefore the sensitivity through the correct choice of probe species. Many of the accompanying effects combine to limit the depth resolution of the technique and must be minimized by correct selection of the primary ion species, energy, and angle of bombardment; and strategies such as reverse-side profiling[5,6] and dual-beam analysis.[7] In the particular case of oxygen bombardment of silicon it is now well-known that bombardment conditions which result in full oxidation minimize the generation of surface topography and that the lowest attainable beam energies result in the best depth resolution.[8] Since the range of incident angle over which the primary beam generates full oxidation increases as the beam energy is reduced, whereas the erosion rate increases with incident angle, there is some flexibility when using sub-kiloelectronvolt oxygen ions to probe the silicon system. We have shown that this flexibility is progressively lost where silicon germanium alloy systems ($Si_{1-x}Ge_x$) are concerned, especially as new generation materials demand $0.5 \leq x \leq 1$, and matrix effects become significant in this range. In this paper, we

Received: November 4, 2011
Accepted: February 1, 2012
Published: February 1, 2012

ACS Publications © 2012 American Chemical Society

explore this problem further and present analysis and quantification methods for ultrahigh depth resolution profiling of $Si_{1-x}Ge_x$ which accounts for both changes in erosion rate and the matrix effects.[9]

Silicon still dominates semiconductor device technology, and normal incidence O_2^+ SIMS depth profiling using a range of primary beam energies spanning many kiloelectronvolts is routinely used to analyze nanometer-scale structures[10,11] in this material. Through recent advances in epitaxial growth, germanium incorporation in silicon to form $Si_{1-x}Ge_x$ alloys across the entire range, i.e., $0 \leq x \leq 1$, has resulted in significant performance improvement over current silicon devices[12,13] while it is also being explored as an alternative to III−V (e.g., GaAs), technologies.[14] However, the SIMS profiles obtained from these alloys using a normal incidence O_2^+ primary beam are far less straightforward to interpret than dopant profiles in bulk silicon and vary greatly with beam energy. Although Ge and Si are in the same group of the periodic table and are fully miscible, their behavior when bombarded with an O_2^+ primary beam is somewhat different. Silicon itself readily oxidizes under O_2^+ bombardment,[15] the net result being a planar, density-renormalized altered layer that is responsible for the high depth resolution obtained, and it is the Si that preferentially oxidizes when $Si_{1-x}Ge_x$ ($x \ll 1$) is bombarded.[16] However, it has recently been shown that for x close to 1, the Ge oxidizes readily for O_2^+ beam energies ≤500 eV.[9] In this energy range, high Ge concentration alloys apparently attain a planarizing surface layer containing Ge oxides, whereas at higher energies the surfaces become rough and lose the potential to achieve the high depth resolution already seen for Si and $Si_{1-x}Ge_x$ at lower values of x.

To investigate this issue further and thereby establish conditions for obtaining accurate and quantifiable depth profiles from samples containing both $Si_{1-x}Ge_x$ and Ge layers, a $Si_{1-x}Ge_x$/Ge multiple quantum well (QW) structure has been studied. Incident beam energies in the range of 0.25−1 keV were used, covering a range of energies believed to be both suitable and unsuitable for profiling Ge. From the resulting profiles we show that low-energy conditions, i.e., ≤ 500 eV, are necessary if profiles representative of the sample structure are to be obtained and the sample matrix concentration determined. Furthermore, because the erosion rate for $Si_{1-x}Ge_x$ ($0 \leq x \leq 1$) varies as a function of x,[9] we have adopted a point-by-point calibration approach for the depth scale by first determining x and then applying an x-dependent erosion rate. The resulting depth scale shows excellent agreement with values obtained using transmission electron microscopy (TEM).

■ EXPERIMENTAL SECTION

The sample designed for this study contained a strained 10 period quantum well structure, with the region of interest having thin (∼14 nm) Ge layers sandwiched between similar thickness (∼11 nm) layers of $Si_{1-x}Ge_x$ (nominal $x = 0.6$). It was grown using an ASM Epsilon 2000 reduced pressure chemical vapor deposition (RP-CVD) tool on a relaxed $Si_{0.2}Ge_{0.8}$ virtual substrate to make the structure strain-balanced, with biaxial compressive strained Ge QWs and biaxial tensile strained $Si_{0.4}Ge_{0.6}$ barriers.[17] Imaging of the sample structure was carried out using cross-sectional transmission electron microscopy (XTEM) using a JEOL 2000FX microscope. Accurate magnification calibration was performed using a III−V superlattice structure with thicknesses measured by high-resolution X-ray diffraction to an accuracy better than 0.01%. Intensity profiles of the images were used to determine individual layer thicknesses; interface positions were taken to lie at the point of maximum gradient in the intensity profile. Ultralow energy secondary ion mass spectrometry (uleSIMS) measurements were carried out using an Atomika 4500 quadrupole instrument which (like other Atomika/Cameca quadrupole instruments) uses ultralow energy gun technology invented at Warwick.[18] A primary O_2^+ beam at near-normal incidence (a condition previously shown to offer the best depth resolution and minimize roughening and pitting[9] in this material) was used over a range of beam energies (0.25−1 keV) with a measured beam current on the sample in the range of 60−100 nA. The primary beam was scanned over an area of 220 μm × 220 μm while both $^{30}Si^+$ and $^{70}Ge^+$ secondary ions were collected. As the sample was intentionally intrinsic (i.e., highly resistive) optical conductivity enhancement (OCE)[19] using a red laser diode (λ = 635 nm; power = 2.5 mW; spot size ∼2 mm at the sample) was employed in order to eliminate any surface potential changes that might have affected the profiles obtained.

Depth calibration was carried out using the procedure outlined below where the total crater depth was measured using a Dektak 3030 stylus profilometer. To minimize errors, the instrument was calibrated immediately prior to use, and each crater was measured six times using two orthogonal sets of three scans distributed across the bombarded region. The average of the scans was then taken to be the crater depth, with the variation about the mean found to be less than ±1%.

Quantification of the uleSIMS Profiles. Conversion of the time and signal intensity values of the SIMS profile for each element to depth and concentration was carried out using the methods implied in ref 9 except that this time x was fitted as a function of ion yield. For the work performed in ref 9, thick (micrometers) constant composition samples quantified by X-ray diffraction (XRD) and spanning the range of $0 \leq x \leq 1$ were profiled using a range of beam energies (0.25−1 keV) with the mean Si and Ge ion yield determined from the signal plateau region (i.e., ignoring the transient region). Plots of ion yield as a function of x indicated that neither ion yield dependence with x could be fitted with a straight line but were pragmatically well-fitted by polynomials. For depth calibration, the erosion rate as a function of x was calculated by dividing the measured crater depths by the profile time for each sample and the erosion rates found were normalized to that found for Si measured at the same energy. Here, only the profiles acquired at ≤500 eV were quantified, as the data for higher energies were inherently unquantifiable, as explained in the next section. The availability of new reference materials with values of x up to 1 meant that the relationships between x and ion yield and x and erosion rate could be established more accurately for the work reported here. It should also be noted that the thin layers within the QW structure were strained, whereas the Si, $Si_{1-x}Ge_x$, and Ge reference samples used were relaxed[9] as the layer thicknesses all exceeded the mechanical equilibrium thickness for strained layer growth.[20]

The concentration is determined first. Note that, for a profile to be quantifiable, the effects of atomic mixing at the interfaces must keep the surface Ge concentration within the range where the Ge signal is monotonically dependent on it. Also, the procedures used here do not attempt to correct for atomic mixing at these interfaces, although the fact that they allow the actual instantaneous surface concentration to be related to the

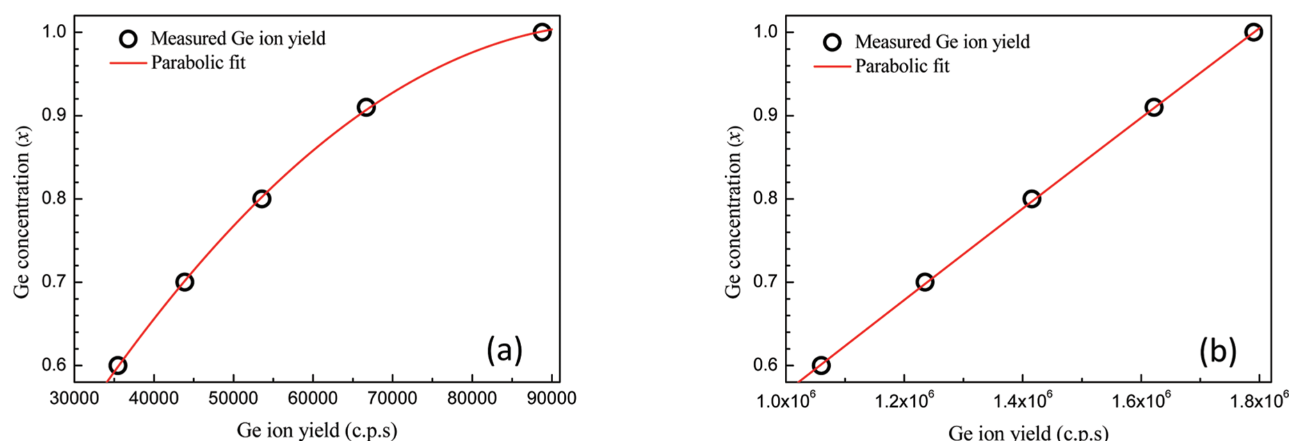

Figure 1. (a and b) Ge concentration (x) as a function of measured Ge ion yield for (a) 250 and (b) 500 eV.

depth corrected for erosion rate changes might facilitate such a correction in future. Parts a and b of Figure 1 show the measured dependence of x on Ge^+ ion yield for 250 and 500 eV, respectively, over a range appropriate to this work determined using Ge fractions of 0.6, 0.7, 0.8, 0.9, and 1.0. The dependence is consistently found to be weakly parabolic in this range:

$$x = X_1(E_p)Y_{Ge} + X_2(E_p){Y_{Ge}}^2 \tag{1}$$

where Y_{Ge} is the measured germanium ion yield and X_n is a primary ion energy E_p dependent coefficient. Table 1a gives the coefficients found and used to quantify x for this work. A cubic dependence is, however, required for the full range of x.[9]

Table 1a. Primary Ion Energy (E_p) Dependent Coefficients Used in Eq 1 for Determining x over the Range of $0.6 \leq x \leq 1$

primary beam energy (eV)	X_1	X_2
250	1.96×10^{-5}	-9.33×10^{-11}
500	5.80×10^{-7}	-1.20×10^{-14}

After the germanium fraction x has been found for the profile of the unknown sample using eq 1, the depth scale is established as follows: The raw data are collected at constant time increment Δt. From measurements of erosion rate relative to bulk silicon ($x = 0$) across the full range of x, a scaling factor s which converts each Δt to an intermediate increment Δt_x is found:

$$\Delta t_{ix} = s(x, E_p)\Delta t_i \tag{2}$$

where the subscript i refers to the ith time increment and

$$s = 1 + ax + bx^2 + cx^3 + dx^4 \tag{3}$$

The coefficients are, once more, beam energy dependent and are given in Table 1b, and the zeroeth-order coefficient is constrained to 1 as the relative erosion rate is 1 when $x = 0$.

Table 1b. Scaling Factor (s) Primary Ion Energy (E_p) Dependent Coefficients Used in Eq 3

primary beam energy (eV)	a	b	c	d
250	0.545	−0.9497	5.07	−3.445
500	0.114	1.86	−0.6079	

Finally, the depth corrected for changes in erosion rate is calculated for the ith value z_i from

$$z_i = \frac{z_m}{t_m}\left(\sum_{n=1}^{i} \Delta t_{nx}\right) \tag{4}$$

where z_m is the measured crater depth and t_m is the actual elapsed time. It is assumed that the shift imposed by the surface transient is negligible at beam energies where the data can be quantified. The determined x values using references may vary by an estimated maximum of ±1 atom %. However, if we were to assume an extreme case where one of the reference ion yields measured at 250 eV were significantly in error, e.g., by ±5%, semiquantitative estimates based on the current data indicate the error in x may increase to ±2.5 atom % at most, depending on which Ge fraction from the set of references was inaccurate. The impact that any variation in x imposes on the depth scale calibration will be dependent on the amount of variation and the complexity of the sample structure being analyzed, i.e., the number of different layers, their x, and thicknesses.

RESULTS AND DISCUSSION

Figure 2 shows a typical (004) XTEM image of the sample with the various $Si_{1-x}Ge_x$ and Ge layers clearly identifiable. Individual layer thicknesses were determined from the intensity profiles (see Table 2). The results indicate that the quantum well layer thicknesses were in reasonable agreement with the designed structure. Two extremely thin lines either side of the QW region are also observed (both in the XTEM and in the SIMS profiles below). These are attributed to surface Ge absorption during growth interrupts resulting in thin regions of increased Ge compared to the surroundings.

Parts a−d of Figure 3 show the raw depth profiles, i.e., ion yield as a function of time, taken from the sample at different beam energies (250, 500, 750 eV, and 1 keV). The Ge profile shape for the Ge layer appears to vary as a function of the beam energy used, with a significant change being observed between those measured at ≤500 eV and ≥750 eV. As the sample structure consisted of Si and Ge only, the expectation might be that, as one of the signals increases, the other should decrease. At 1 keV (Figure 3a) this is certainly not the case while the near-square profile expected for the Ge signal was also not observed. Closer inspection of the profile reveals that as the beam reaches the Ge layer, the Ge signal begins to rise as expected. However, before reaching a plateau the signal

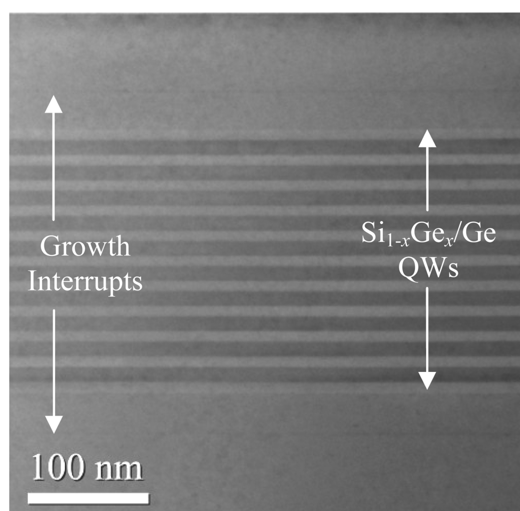

Figure 2. Cross-sectional transmission electron microscopy (XTEM) image of the $Si_{1-x}Ge_x$/Ge sample.

suddenly falls (as highlighted in Figure 3a), before rising and stabilizing again as the beam reaches the next $Si_{0.4}Ge_{0.6}$ layer. This behavior repeats itself at each Ge layer and is indicative of a reduced Ge^+ ionization probability as previously observed and reported for thick (micrometer-scale) Ge layers measured at this energy and higher.[21,22] For 750 eV (Figure 3b), the Ge signal also shows some distortion within the Ge layers, although not as severe as that seen at 1 keV. Again this is believed to be due to an inadequate Ge^+ ionization, with the net result for both energies being an unrepresentative and unquantifiable profile.

For the ≤500 eV profiles (Figure 3, parts c and d), the Si and Ge signal behavior is more as expected; the Si signal drops as the Ge signal increases and vice versa for the regions of compositional variation, whereas both remain flat for the constant composition regions. This suggests that good probe–sample interaction conditions are now being achieved and maintained as we profile through the different compositions. Furthermore, the monotonic variation of ion yield with Ge concentration[9] means that the latter quantity can be extracted as shown in eq 1.

As well as determining the atomic concentration of the individual layers, a fully quantified depth profile also requires an accurate depth scale. The simplest type of sample to depth calibrate is one with a single matrix. This is because if equilibrium profiling conditions are reached, i.e., after the initial transient region,[23] a constant erosion rate is achieved. A depth scale is then applied by measuring the depth of the crater and then converting the profile time taken into this measured depth. This method is typically very accurate so long as the transient region is small compared to the total profile depth. However, this approach will break down when the sample contains numerous layers of differing matrix composition because the erosion rate will inevitably vary with composition, so an approach such as that described by eqs 2–4 becomes essential. (It is worth noting that a rather similar approach was devised by Clark[24] for GaAs/AlGaAs multilayers in as early as 1986.)

Parts a and b of Figure 4 show the fully quantified (concentration and depth calibrated) 250 and 500 eV profiles,

Table 2. Intended Layer Composition and Thicknesses, Together with Thicknesses Determined from XTEM and from 250 and 500 eV uleSIMS Depth Profiles Quantified Using a Constant Erosion Rate (ER(const)) and a Point-by-Point Erosion Rate as a Function of x (ER(x))[a]

				250 eV uleSIMS		500 eV uleSIMS	
layer	intended layer composition	intended layer thickness (nm)	XTEM layer thickness (nm)	ER(const) thickness (nm)	ER(x) thickness (nm)	ER(const) thickness (nm)	ER(x) thickness (nm)
1	$Si_{0.2}Ge_{0.8}$	100	97 ± 2	101 ± 2	102 ± 2	103 ± 2	102 ± 2
2	$Si_{0.4}Ge_{0.6}$	11	8.6 ± 0.5	9.7 ± 0.5	8.7 ± 0.5	10.2 ± 0.5	8.7 ± 0.5
3	Ge	14	12.6 ± 0.5	11.5 ± 0.5	12.7 ± 0.5	11.3 ± 0.5	12.8 ± 0.5
4	$Si_{0.4}Ge_{0.6}$	11	8.6 ± 0.5	9.7 ± 0.5	8.5 ± 0.5	10.3 ± 0.5	8.7 ± 0.5
5	Ge	14	12.7 ± 0.5	11.5 ± 0.5	12.7 ± 0.5	11.1 ± 0.5	12.5 ± 0.5
6	$Si_{0.4}Ge_{0.6}$	11	8.6 ± 0.5	9.7 ± 0.5	8.7 ± 0.5	10.4 ± 0.5	9.0 ± 0.5
7	Ge	14	12.6 ± 0.5	11.5 ± 0.5	12.6 ± 0.5	11.0 ± 0.5	12.4 ± 0.5
8	$Si_{0.4}Ge_{0.6}$	11	8.5 ± 0.5	9.6 ± 0.5	8.6 ± 0.5	10.4 ± 0.5	9.0 ± 0.5
9	Ge	14	12.6 ± 0.5	11.5 ± 0.5	12.6 ± 0.5	11.1 ± 0.5	12.4 ± 0.5
10	$Si_{0.4}Ge_{0.6}$	11	8.5 ± 0.5	9.7 ± 0.5	8.6 ± 0.5	10.2 ± 0.5	8.8 ± 0.5
11	Ge	14	12.7 ± 0.5	11.6 ± 0.5	12.7 ± 0.5	11.2 ± 0.5	12.6 ± 0.5
12	$Si_{0.4}Ge_{0.6}$	11	8.5 ± 0.5	9.5 ± 0.5	8.6 ± 0.5	10.1 ± 0.5	8.7 ± 0.5
13	Ge	14	12.7 ± 0.5	11.3 ± 0.5	12.5 ± 0.5	11.1 ± 0.5	12.4 ± 0.5
14	$Si_{0.4}Ge_{0.6}$	11	8.4 ± 0.5	9.7 ± 0.5	8.6 ± 0.5	10.3 ± 0.5	8.9 ± 0.5
15	Ge	14	12.7 ± 0.5	11.5 ± 0.5	12.7 ± 0.5	11.1 ± 0.5	12.4 ± 0.5
16	$Si_{0.4}Ge_{0.6}$	11	8.5 ± 0.5	9.8 ± 0.5	8.9 ± 0.5	10.4 ± 0.5	9.0 ± 0.5
17	Ge	14	12.7 ± 0.5	11.4 ± 0.5	12.5 ± 0.5	11.0 ± 0.5	12.4 ± 0.5
18	$Si_{0.4}Ge_{0.6}$	11	8.4 ± 0.5	9.9 ± 0.5	8.8 ± 0.5	10.6 ± 0.5	9.0 ± 0.5
19	Ge	14	13.0 ± 0.5	11.5 ± 0.5	12.7 ± 0.5	11.1 ± 0.5	12.4 ± 0.5
20	$Si_{0.4}Ge_{0.6}$	11	8.6 ± 0.5	10.0 ± 0.5	8.9 ± 0.5	10.6 ± 0.5	9.0 ± 0.5
21	Ge	14	12.8 ± 0.5	11.7 ± 0.5	12.7 ± 0.5	11.3 ± 0.5	12.5 ± 0.5
22	$Si_{0.4}Ge_{0.6}$	11	9.0 ± 0.5	10.2 ± 0.5	9.2 ± 0.5	10.5 ± 0.5	9.6 ± 0.5

[a]NB: layer 1 nearest the surface.

dx.doi.org/10.1021/ac202929x | Anal. Chem. 2012, 84, 2292–2298

Figure 3. (a−d) Raw uleSIMS depth profiles of the $Si_{1-x}Ge_x$/Ge quantum well sample measured using normal incidence O_2^+ at (a) 1 keV and (b) 750, (c) 500, and (d) 250 eV.

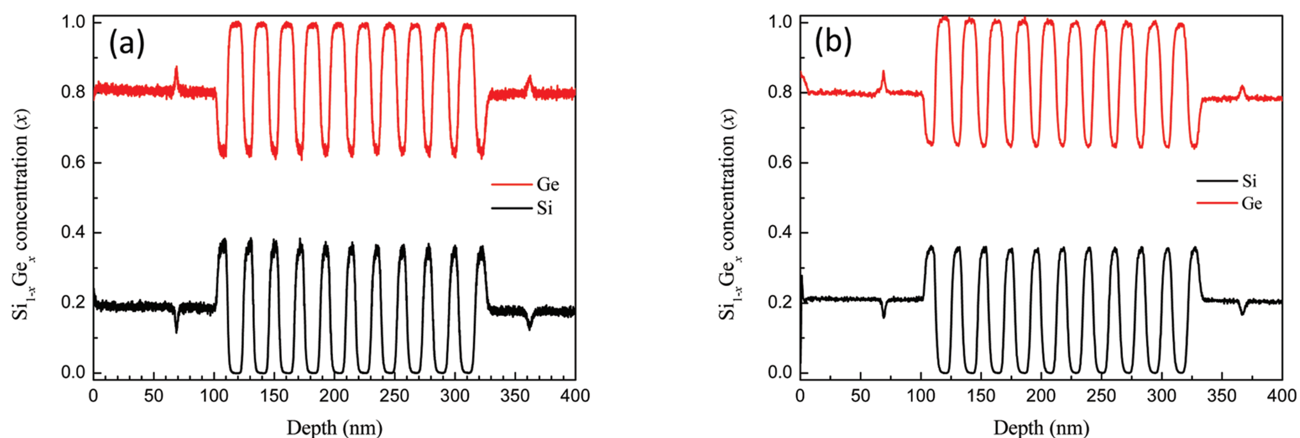

Figure 4. (a and b) Quantified uleSIMS depth profiles of the $Si_{1-x}Ge_x$/Ge quantum well sample profiled using O_2^+ at normal incidence and (a) 250 and (b) 500 eV.

respectively. From these profiles, the Ge concentration determined for the various layers throughout the sample is in excellent agreement with previously reported values for this sample which were ascertained by X-ray diffraction.[17] The QW layer thicknesses were also estimated by using the full width at the midpoint of the Ge signal, i.e., ~82 atom % Ge, because this point was similar to that used from the XTEM images to establish layer thicknesses. A summary of the uleSIMS findings is given in Table 2.

For comparison, and to demonstrate the effect of incorrect depth scaling, the depth scale of the 250 eV and 500 eV profiles were evaluated using a single erosion rate which is typically

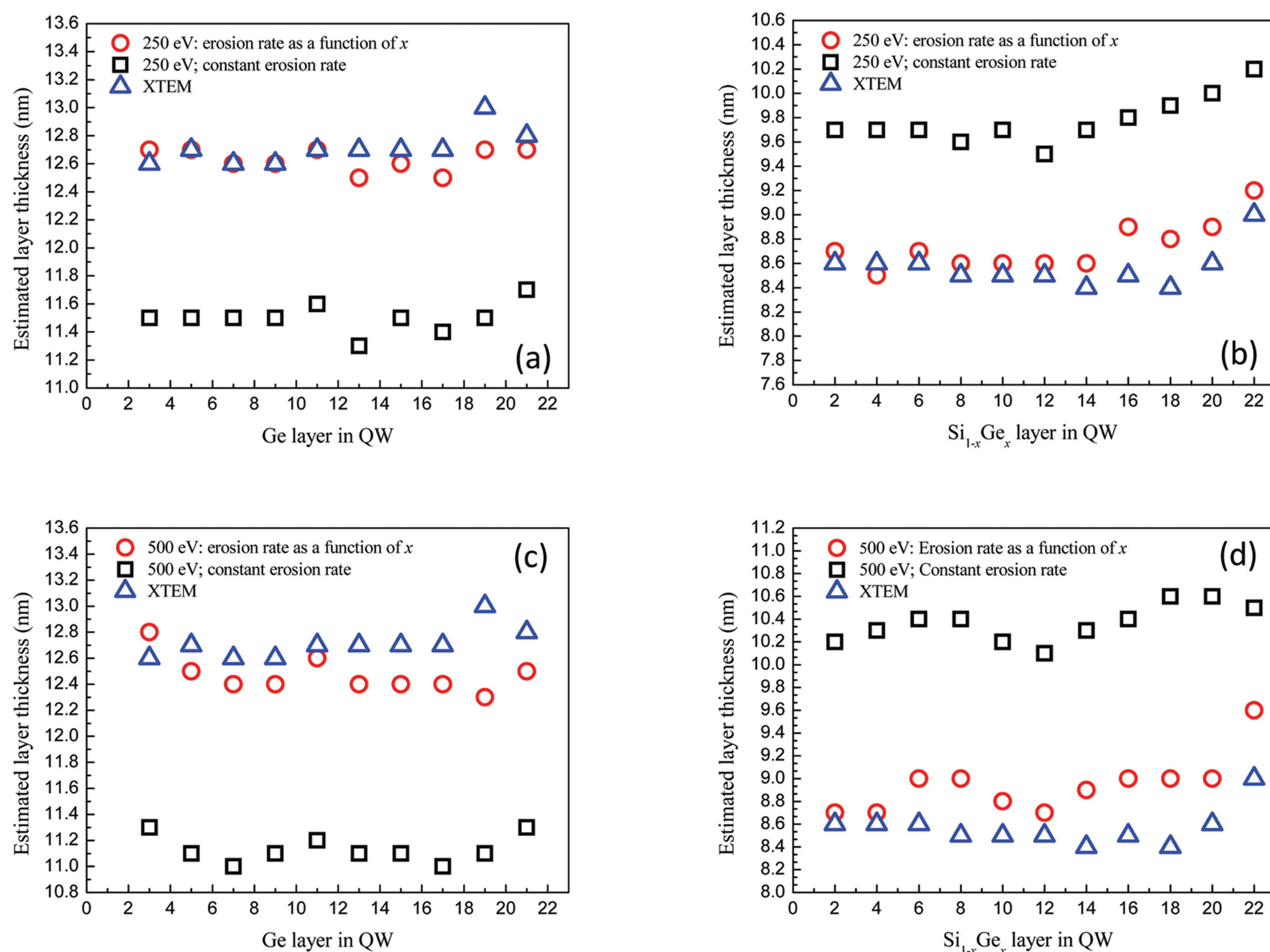

Figure 5. (a–d) Plots showing the estimated quantum well layer thicknesses ($Si_{1-x}Ge_x$ and Ge) taken from the quantified uleSIMS profiles using ER(const) and ER(x) and from XTEM: (a) 250 eV Ge layer thicknesses, (b) 250 eV $Si_{1-x}Ge_x$ layer thicknesses, (c) 500 eV Ge layer thicknesses, and (d) 250 eV $Si_{1-x}Ge_x$ layer thicknesses.

used for single matrix materials. The estimated layer thicknesses from these profiles are also given in Table 2. Parts a–d of Figure 5 compare the estimated $Si_{1-x}Ge_x$ and Ge quantum well layer thicknesses obtained from the 250 and 500 eV profiles for both a constant erosion rate (ER(const)) and the point-by-point approach (ER(x)) against those determined by XTEM. In the case of ER(const), it is seen that the $Si_{1-x}Ge_x$ and Ge layer thicknesses are over- or underestimated, by up 16%, compared to the XTEM, whereas excellent agreement is found where the erosion rate (ER(x)) has been taken into account, with the 250 eV ER(x) data appearing to offer slightly better agreement compared with the 500 eV ER(x) data. The small difference between these energies is believed to be a consequence of the increased atomic mixing at 500 eV which leads to a slight broadening of the layer interfaces. The large discrepancy between ER(const) and the XTEM is unsurprising based on the erosion rate behavior now known for $Si_{1-x}Ge_x$ ($0 \leq x \leq 1$). Moreover, the scale of this discrepancy would clearly increase proportionately for thicker layers.

CONCLUSIONS

Probe energies ≤500 eV at near-normal incidence are required to obtain accurate quantification of x from a $Si_{1-x}Ge_x$/Ge multilayer sample and an accurate depth scale. For energies ≥750 eV and x approaching 1, a reduced Ge^+ ionization probability results in unrepresentative and unquantifiable depth profiles. At energies ≤500 eV a monotonic variation of Ge ion yield with x is found, resulting in profiles from which the sample structure can be extracted by first finding x using an energy-dependent yield function and then establishing the depth scale from an x and energy-dependent erosion rate point by point, with both being established from relaxed reference materials. The concentrations and thicknesses of the various layers determined using these methods are found to be in excellent agreement with concentrations previously reported for this sample using XRD[17] and thicknesses determined using XTEM. The use of a single erosion rate is shown to over- and underestimate the $Si_{1-x}Ge_x$ and Ge layer thicknesses, respectively.

AUTHOR INFORMATION

Corresponding Author

*E-mail: r.morris@warwick.ac.uk.

Notes

The authors declare no competing financial interest.

ACKNOWLEDGMENTS

This work was supported by the EPSRC through the U.K. Silicon Photonics and Renaissance Ge projects. The Gatan Orius digital TEM camera used in this research was funded by the Advanced Materials (1) project: Creating and Characterising Next Generation Advanced Materials, part funded by

Advantage West Midlands and the European Regional Development Fund.

REFERENCES

(1) Williams, P. *Surf. Sci.* **1979**, *90*, 588−634.
(2) Littmark, U.; Hofer, W. O. *Nucl. Instrum. Methods* **1980**, *168*, 329−342.
(3) Jiang, Z. X.; Alkemade, P. F. A. *Appl. Phys. Lett.* **1998**, *73*, 315−317.
(4) Wittmaack, K. *Nucl. Instrum. Methods Phys. Res., Sect. B* **1987**, *19/20*, 484−487.
(5) Shappirio, J. R.; Lareau, R. T.; Lux, R. A.; Finnegan, J. J.; Smith, D. D.; Heath, L. S.; Taysing-Lara, M. *J. Vac. Sci. Technol., A* **1987**, *5*, 1503−1507.
(6) Gu, G.; Garcia, R.; Pivovarov, A.; Stevie., F.; Griffis, D. *Appl. Surf. Sci.* **2004**, *231−232*, 663−667.
(7) Iltgen, K.; Bendel, C.; Benninghoven, A.; Niehuis, E. *J. Vac. Sci. Technol., A* **1997**, *15*, 460−464.
(8) Dowsett, M. G. *Fresenuis' J. Anal. Chem.* **1991**, *341*, 224−234.
(9) Morris, R. J. H.; Dowsett, M. G. *J. Appl. Phys.* **2009**, *105*, 114316.
(10) Dowsett, M. G.; Barlow, R. D.; Fox, H. S.; Kubiak, R. A. A. *J. Vac. Sci. Technol., B* **1992**, *10*, 336−341.
(11) Vandervorst, W.; Sheppard, F. R. *J. Vac. Sci. Technol., A* **1987**, *5*, 313−320.
(12) Whall, T. E.; Parker, E. H. C. *Thin Solid Films* **2000**, *367*, 250.
(13) Morris, R. J. H.; Grasby, T. J.; Hammond, R.; Myronov, M.; Mironov, O. A.; Leadley, D. R.; Whall, T. E.; Parker, E. H. C.; Currie, M. T.; Leitz, C. W.; Fitzgerald, E. A. *Semicond. Sci. Technol.* **2004**, *19*, L106−L109.
(14) Kang, Y.; Han-Din, L.; Morse, M.; Paniccia, M. J.; Zadak, M.; Litski, S.; Sarid, G.; Pauchard, A.; Kuo, Y.-H.; Chen, H.-W.; Zaoui, W. S.; Bowers, J. E.; Beling, A.; McIntosh, D. C.; Zheng, X.; Campbell, J. C. *Nat. Photonics* **2009**, *3*, 59−63.
(15) Clark, E. A.; Dowsett, M. G.; Spiller, G. D. T.; Thomas, G. R.; Augustus, P. D.; Sutherland, I. *Vacuum* **1988**, *38*, 937−941.
(16) Coster, W. D.; Brijs, B.; Vandervorst, W. *Proceeding of the Tenth Secondary Ion Mass Spectrometry Conference*; Benninghoven, A., Hagenhoff, B., Werner, H. W., Eds.; John Wiley & Sons: Chichester, West Sussex, UK, 1995; p 529.
(17) Liu, X.-C.; Morris, R. J. H.; Myronov, M.; Dobbie, A.; Leadley, D. R. *J. Phys. D: Appl. Phys.* **2011**, *44*, 079501.
(18) Dowsett, M. G.; Smith, N. S.; Bridgeland, R.; Richards, D.; Lovejoy, A. C.; Pedrick, P. *Proceeding of the Tenth Secondary Ion Mass Spectrometry Conference*; Benninghoven, A., Hagenhoff, B., Werner, H. W., Eds.; John Wiley & Sons: Chichester, West Sussex, UK, 1995; p 367.
(19) Morris, R. J. H.; Dowsett, M. G.; Chang, R. J. H. *Appl. Surf. Sci.* **2006**, *252*, 7221−7223.
(20) Matthews, J. W.; Blakeslee, A. E. *J. Cryst. Growth* **1974**, *27*, 118−125.
(21) Morris, R. J. H.; Dowsett, M. G. *Surf. Interface Anal.* **2011**, *43*, 543−546.
(22) Huyghebaert, C.; Conard, T.; Brijs, B.; Vandervorst, W. *Appl. Surf. Sci.* **2004**, *231−232*, 708−712.
(23) Krüger, D.; Efremov, A. A.; Murota, J.; Kups, R.; Bugiel, E.; Tillack, B.; Romanova, G. P. *Surf. Interface Anal.* **2002**, *33*, 663−671.
(24) Clark, E. A. *Vacuum* **1986**, *36*, 861−863.